Research Article

# A Study on Various Common Denoising Methods on Chest X-ray Images

**Subhagata Chattopadhyay** (ID)

Independent researcher, Bangalore 560098 Karnataka India
Email: subhagata.chattopadhyay2017@gmail.com

**Abstract:** Image 'denoising' is an important pre-processing step as noise affects the image quality. The behaviors of denoising algorithms have been examined on a set of 2D Chest X-ray (CXR) images. Both the 'Linear' and 'non-Linear' denoising methods are considered, each having two techniques, such as (i) *Moving average* and (ii) *Gaussian* under the Linear method, and (iii) *Median* and (iv) *Bilateral* under the non-Linear method, respectively. *Noise variance and Signal-to-Noise Ratio (SNR)* are computed on the raw images. The study finds that, *Median filter* is the best of the lot with the PSNR mean = 34.5213; PSNR $\sigma$ = 0.9618; MSE mean = 12.2337; MSE $\sigma$ = 1.5491; and Big(O) = 0.02873 milliseconds. Finally, a comparative study has been made among these denoising methods to predict five hundred Tubercular CXRs, which shows that, using the Median filter, 92% CXRs can be accurately diagnosed, followed by Gaussian, Bilateral, and Moving average type filters with the respective accuracies of 80%, 72%, and 60%, respectively. This work could be a ready-reckoner to the researchers in choosing the best filtering technique when working on Medical X-ray images.

*Keywords*: medical image processing, chest X-ray image, image filtering, computational complexity

## 1. Introduction

Images are usually found corrupted with different types and grades of noise within it. Variation in the brightness of an image is considered noise [1]. Degrees of variations determine the level of noise in an image. The presence of 'Noise' is due to various reasons, such as instrumental defects, interference of media such as water droplets (moisture) in the air and airflow speed, over or under exposure of light, acquisition and development-related issues, image transmission, dead pixels and so forth [2-3]. The presence of noise, therefore, is a natural phenomenon and not a fallacy. To efficiently process an image, noise reduction is one of the priority steps, as low noise renders high-quality images, which could be achieved by removing or modifying the bad quality and or redundant pixels. In today's era, applications of Machine Learning (ML) and Artificial Intelligence (AI) in Image processing are gaining tremendous speed to automate diagnostic and prognostic decision-making by the machines, which are trained by ML/AI algorithms [4-6]. Clustering methods have been extensively used to segment the chest CT images of COVID-19 cases [7-8]. In healthcare, doctors depend on radiological investigations, such as X-rays, Ultrasonography (USG), Doppler scans, Computerized Tomogram (CT), Magnetic Resonance Imaging (MRI), functional Magnetic Resonance Imaging (fMRI), Mammography,

Angiography, Positron Emission Tomography (PET), Single Photon Emission Computerized Tomography (SPECT), etc. for diagnostic, therapeutic and prognostic purposes [9]. Compared to the rest, *X-rays* are an economic and popular radiological modality, used vastly in clinical setups. Photons with a wavelength of less than 0.2 to 1.0 nm produce X-rays and have high tissue penetration power. Currently, X-ray images are produced by a digital receptor [10]. Due to its higher volume of X-ray images each hour and the lack of an adequate number of qualified radiologists in healthcare setups, automatic techniques are encouraged to assist medical doctors in critical decision-making [11-12]. The quality of accuracy and precision of such an automatic diagnosis of any radiological image depends on its quality and therefore needs to be pre-processed to reduce the noise level before being processed under ML/AI algorithms. Therefore, a medical image needs to be appropriately pre-processed as a mandatory measure in the current day's image processing research [13].

There are several types of *Noise* in the image, such as *Amplifier noise*, *Impulsive or Salt and pepper or Spike noise*, Poisson noise, and *Speckle noise* [10, 14]. Principally there are two types of noise models, such as *additive* (see equation 3a) and *multiplicative* (see equation 3b) [14]. *The amplifier* noise model is typically an additive or Gaussian or independent of each pixel or signal intensity [14]. In color images, amplification happens mostly on the blue color channel than that of red and green. Hence, more amplifier noise can be found in the blue channel [15]. In an image sensor, the amplifier is the major type of noise with Gaussian distribution and is consistently found in the dark areas of an image [14]. *Impulsive noise* is found in the areas where dark pixels are found in bright areas and *vice versa* and is more commonly seen in radiographic images [14]. The reasons could be transmitted bit errors or analog-to-digital conversion errors [14]. This type of noise can be measured by computing the ratio of the mean of the dynamics of the gray levels of a homogeneous region to the maximum value of that region when the ratio value exceeds the preset threshold value [14]. *Speckle noise* is a type of multiplicative means of noise. It is commonly found in radar images as granular noise degrades the image quality. Speckle noise increases the mean gray level of the local area in an image [14].

*Denoising* is an important prerequisite to any image processing method. There are three principal denoising methods available, such as *Spatial filtering*, *Transform Domain Filtering*, and *Wavelet Thresholding Method* [14]. The key objectives of applying these methods are to suppress/reduce/eliminate noise in any given region of the image, preserve important features of the image, such as edge, depth, contrast, brightness, etc., and render a visually natural appearance of the image, which can be perceived and appreciated by the occipital cortex (called as the visual cortex) of the brain. In this work, the Spatial filtering method has been used and hence, other methods are skipped in this section.

*Spatial filters* are traditional denoising techniques and work nicely when only additive noise is present [14]. It is sub-classified into two methods, such as *Linear* and *Non-linear* filters. Under Linear filters, there are three popular techniques, e.g., *mean/average* filtering technique, *Gaussian* filtering technique, and *Weiner* filtering technique [14]. In this work, the first two techniques have been used under the Linear filtering method. Non-Linear Filters are used when multiplicative and function-based noise exists in an image [14]. Under the Non-Linear Filtering method, *Median* and *Bilateral* filtering techniques are used in this study. The working principles of Average, Gaussian, Median, and Bilateral filtering techniques are described in Section 2.

In the next section, a detailed literature survey focused on applications of various denoising techniques on radiographic images has been conducted to highlight a large sample of works on various denoising/filtering methods used in medical radiographs. It is important to mention here that this list of research work is not an exhaustive one and there are many more works in the database. However, due to space constraints, all cannot be mentioned in this work.

# 2. Literature review

In this section, research works on the applications of the above-mentioned four denoising techniques, such as *Average*, *Gaussian*, *Median* and *Bilateral* filters, used in this work are discussed and the rest are skipped for not falling into the scope of this work. The area of application is focused on medical images. The concise table below (Table 1) showcases the relevant and important aspects of the studies.

**Table 1.** Summary of the literature review

| Author | Filter type | Radiograph type | Discussion |
|---|---|---|---|
| [16] | Median (improved) | MRI brain | The improved algorithm works better on salt and pepper type of noise compared to conventional median filter by detecting noise and establishing noise marked matrix and does not process pixels as signals. |
| [17] | Median filter-2D and 3D Simple and Fermat methods, each | DT-MRI neuronal fiber bundles | All four techniques can regularize DT-MRI tactograms efficiently with less computational time. |
| [18] | Median (modified), Minimum, Maximum, Gaussian, and Average | MRI brain and spinal cord | The modified Median filter outperformed the other filtering methods. |
| [19] | Median (modified) | MRI brain | The adaptive median filter is the best salt and pepper denoising technique |
| [20] | Median | MRI heart | Able to eliminate impulse, fluctuation, and geometric noise. |
| [21] | Average, Median, Weiner | CT lungs | The median filter outperformed Average and Weiner filtering techniques to eliminate noise as evidenced by low MSE and high PSNR values. |
| [22] | Adaptive Median Filter (AMF) and Wavelet Packed Threshold Shrinkage (APTS) | CT lungs | AMF can reduce salt and pepper and Gaussian noise in the CT images. |
| [23] | Median | CT lungs | The median filter can efficiently eliminate noise from the image. |
| [24] | Median2, Imadjust, Weiner, tophat, bothat | 2D CXR | The combination of all filters can denoise the images and be able to successfully detect chest Tuberculosis. |
| [25] | Adaptive, Median, and Bilateral | CXR | Both filters can suppress Gaussian noise and Impulsive noise effectively. |
| [10] | Responsive and Simple Median filtering (SMF) and Moving Average (MA) filtering | CXR | The responsive Median filter outperforms the SMF and AF techniques. |
| [26] | Bilateral filter weighted by Gaussian filtered sinogram (BFWGFS) | Low-dose X-ray Computed Tomogram (LDCT) | BFWGFS technique can eliminate the noise values due to various artifacts. |
| [27] | Median, Average, and Adaptive | CXR, MRI | An adaptive filter works better to denoise Gaussian noise in X-ray and MRI images. |

*Scope of the research:* From the above studies, it can be noted that the *Median filter* and its several variations work nicely in denoising medical images, such as MRI, CT, X-rays, etc. This work is to re-examine the efficacy of a *Simple Median Filter* on a set of *CXR radiographs* and compare its denoising performances against three other closely associated techniques, such as *Moving average*, *Gaussian*, and *Bilateral* filters by computing various noise measuring formulae.

The rest of the paper is structured as follows:

Section 3 describes the material and methods, while Section 4 showcases the results and explains them appropriately; finally, Section 5 draws conclusions from this experiment and directs the scope of future work.

# 3. Material and methods

In this section, the material and experimental methods of the study have been discussed. Figure 1 shows the flow diagram of the experiment. Each method is then described.
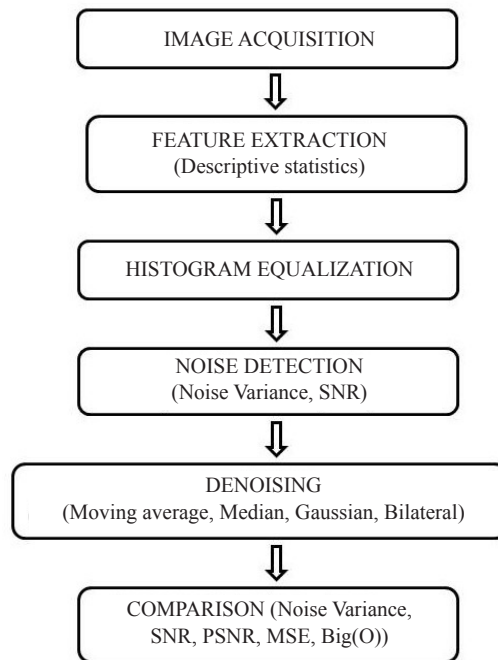
**Figure 1.** Flow diagram of the methodology

## 3.1 *Material-CXR images*

Three *Chest X-rays (CXR)* of adult males have been acquired from an X-ray clinic. One of these is 'normal' and has been termed as a 'Control' image; while the other two are pathological and are termed as 'Test CXR-1' and 'Test CXR-2' (refer to Figure 3). Other than catering to the variations among the image datasets, this variety is not meant for image classification or diagnosis of any type. *Ethical measures*, such as patients' names, Medical Record (MRD) numbers, and the name of the source clinic have been kept anonymous throughout the study.

*Methods* (mentioned through *B to G)*, used in this study, are described below step-by-step.

## 3.2 *System information*

All coding for the experiment has been conducted on *Python 3.8.3* with *Spyder* editor version 4.1.5, preloaded with matplotlib, skimage, numpy, OpenCV, and pandas. All computations are primarily run on *Windows 10 Pro 64 bits OS×64-based Processor Intel(R) Core TM @ 2.80 GHz*.

## 3.3 *Feature extraction*

The feature or texture of any dataset provides insight into the data [28]. Hence, feature extraction poses an important step in data mining to retrieve meaningful and interesting patterns in the size and shape of the data and varieties within [29]. Descriptive statistics, which includes Mean, Max value, Min value, Quartile or Q values-Q1, 2 or Median, and 3, Standard deviation is the most basic but highly informative statistical data mining technique to obtain enough light on the nature and distribution of any data [30]. Another important parameter is the 'Skewness' of the data [31]. It is an estimation of data distribution and its direction. In case of the probability distribution is curved towards the right side, the data is said to be positively skewed and vice versa. In image data, descriptive data analysis is done on the pixel values (see Table 2).

In this work, three CXR images have been considered for study-one normal (called Control) and two pathological (called CXR Test-1 and CXR Test-2). These image datasets are desired to be varied in nature to test the performances of the denoising techniques.

Next, in the experiment, to enhance the image qualities, Histogram Equalization (HE) has been performed on each of the CXR images and is described below.

## 3.4 *Histogram equalization/linearization*

Human eyes are most sensitive to the contrast of an image. We perceive images in the visual cortex of our brain based on the degree of 'high-density distribution', i.e., high contrast through which we can gather more meaningful information about an image, compared to low or poor density distribution or contrast of an image where information is masked due to lower density values, which are not well-appreciated by the brain. Histogram equalization (HE) is a popular technique by which 'contrast' can be enhanced effectively by spreading out the most frequent intensity values of an image. It is therefore a method of stretching or adjusting the intensity range of the image (refer to Figure 2, where most frequent intensity pixel values are marked by Red color and relatively less frequent intensity pixel values are marked by blue color).
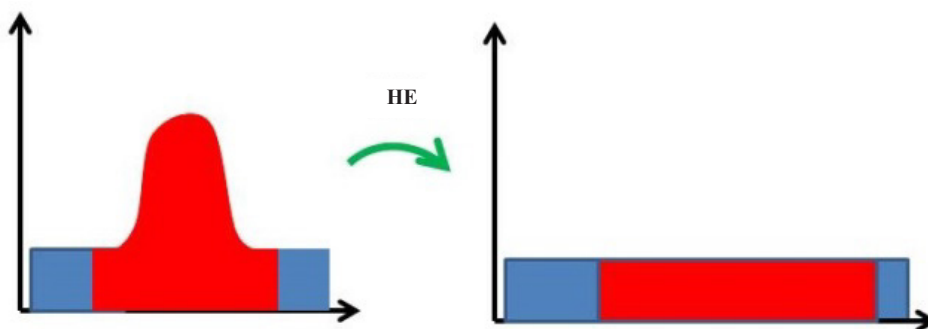
**Figure 2.** The concept of HE-original image (left) and after HE (right)

In a comprehensive study, the authors mentioned that HE can increase the global contrast of many images, especially when the usable data of the image is represented by close contrast values. By doing this adjustment, the intensities can be better distributed on the histogram along its x-axis due to the stretching. Such a distribution allows areas of lower local contrast (marked by Blue color in Figure 1) to gain higher contrast values, marked by red color [32]. By enhancing the contrast, it can enrich the image quality, but not always. In some instances, Histogram Equalization (HE) leads to a worsening of the image quality. It is not always a unique representative of an image, which means that multiple images may have the same histogram.

HE is represented as a graph of pixel gray level values (along the x-axis) and their corresponding intensities/frequencies (along the y-axis), which can be noted in Figure 3.

A histogram of a continuous random variable is often called a '*Probability Distribution Function (PDF)*'. The area under a PDF (which is a definite integral) is called a '*Cumulative Distribution Function (CDF)*'. The CDF quantifies the probability of observing certain pixel intensities. CDF computes the cumulative probability for a given 'x' value (i.e., a pixel value). It has three important properties, (i) it is a non-decreasing function, (ii) for 'x' (any random variable) tends to -∞ (minus infinity), CDF of 'x' approaches 0.0, and (iii) for 'x' (any random variable) tends to ∞ (plus infinity), CDF of 'x' approaches to 1.0.

*The Working principle* of HE [33] is expressed as a discrete function '$h(rk) = nk$', where '$rk$' is the $k^{th}$ gray level ($k$ = 0 to $L-1$) in the range of $[0, L-1]$ and '$nk$' is the number of pixels having '$rk$' gray levels. '$L$' is the total number of gray levels, which is 255. As mentioned above, it stretches the dynamic range of the gray levels in a low-contrast image to consider the full range of all gray levels. For pixel '$x$', the intensity value after equalization would be:

$$I(x) = round[cdf(x) - \min(cdf)/1 - \min(cdf)] \times (L-1) \tag{1}$$

$$cdf[k] = \sum_{j=0}^{k} 255^{n_j} / N \tag{2}$$

In equations 1 and 2, '*cdf*[*k*]' is the *Cumulative Density Function (CDF)* of the pixel with value '*k*' in the input image, which is the number of pixels with value '*j*' and '*N*' is the total number of pixels.

Finally, all input pixels are *relabeled* with corresponding values of '*cdf*[*k*]' in the equalized image or contrast-enhanced image. Contrast stretching along the x-axis abreast '*cdf*' line plots can be seen in Figure 3 below.

By applying the HE technique, the contrast of each of the three CXR images has been enhanced to examine if there is any chance of noise reduction before the actual denoising tasks. This is the *rationale* for using the HE in this work.

## 3.5 *Noise detection*

*Noise* is an important factor that is responsible for the quality of any image. It can be induced in various ways, such as the discrete nature of radiation, variation in detector sensitivity, photographic gain effect, properties of image systems (e.g., air turbulence), modalities of images, data transmission errors, and so on [34]. There are different types of noises, such as Salt and pepper, Gaussian, Poisson, Impulse, Speckle, and so on [35].

Noise in an image can be found in two major forms-(i) *Additive term* (refer to equation 3a) and (ii) *Multiplicative term* (refer to equation 3b).

In this work, noise in the images is calculated by two following techniques:

### 3.5.1 *Noise variance*

If an image $f(i, j)$ is scaled by *additive terms* '*a*' and '*b*', to give

$$g(i, j) = af(i, j) + bf(i, j) \tag{3a}$$

If an image $f(i, j)$ is scaled by the *multiplicative* factors '*a*' and '*b*', to give

$$g(i, j) = af(i, j) \tag{3b}$$

In this study, additive terms have been used as shown in equation (3c),

$$g(i, j) = af(i, j) + b \tag{3c}$$

then, the *mean* of $g(i, j)$ is given by,

$$g = af + b \tag{4}$$

then, the *variance* of $g(i, j)$ is given by,

$$\sigma_g^2 = a^2 \sigma_f^2 \tag{5}$$

Where, $\sigma_f^2$ is the noise variance of image $f(i, j)$. Therefore, the value decreases with a low noise level.

After computing the noise variance, the *Signal-to-Noise Ratio (SNR)* has been computed, as follows.

### 3.5.2 *Signal-to-Noise Ratio (SNR)*

It is estimated as shown in equation (6), below

$$f(i, j) = s(i, j) + n(i, j), \tag{6}$$

then, *variances* of $s(i, j)$ and $n(i, j)$ can be written as (equations 7 and 8), below

$$\sigma_s^2 = \left\{ \,|\, s(i, j) - s(i, j) \,|^2 \right\}, \tag{7}$$

and

$$\sigma_n^2 = \left\{ n(i, j)^2 \right\} \tag{8}$$

and then finally *SNR* can be written as equation (9),

$$SNR = \frac{\sigma_s}{\sigma_n}. \tag{9}$$

Therefore, *SNR* is a ratio of true signal (*s*) and additive noise (*n*). The value increases with a low noise level.

In the experimental results section, the values thus obtained for the images have been shown in Table 3a (raw images before HE application) and Table 3b (HE applied images).

## 3.6 *Image denoising (kernel size 5×5)*

Automated diagnosis of medical images is the current trend. To achieve the highest quality of results, i.e., precision and accuracy, image denoising is an essential step. In this study, two linear and two non-linear filtering techniques have been used. The working principles of each technique are explained and in turn, their performances are compared.

The detail of the *working principles* of the denoising techniques:

*a) Moving Average* (type: linear filter)-it is a linear convolution where images under pre-processing can be smoothened by reducing the number of intensity variations between neighboring pixels by calculating running averages of the neighboring pixels in a finite series. It moves pixel-by-pixel and replaces each value (including its value) by calculating the *average* of the neighborhood pixel. The disadvantage of this type of filter is that presence of any single unrepresentative pixel having high entropy from the rest of the pixels may influence the average value throughout the value-updating task in the image under study. There are three popular types of Moving averages, such as (i) Simple, (ii) Cumulative, (iii) Exponential, and (iv) Weighted moving averages. In this work, *Simple Moving Average (SMA)*, which is also called a Boxcar Filter, has been applied. The working principle of an SMA algorithm is as follows [36], and can be written as shown in equations (10a) and (10b), below,

$$SMA_k = \frac{1}{k} \sum_{i=n-k+1}^{n} p_i \tag{10a}$$

Where '$k$' refers to the last entered pixel datasets having $p_i$ number of pixel data points in '$n$' number of entries; '$i$' represents the data range', then $SMA_{k\_next}$ can be calculated as,

$$SMA_{k\_next} = \frac{1}{k} \sum_{i=n-k+2}^{n+1} p_i \tag{10b}$$

*b) Median* (type: non-linear filter)-where output value is computed based on the *median* value of the input sample and then sorted. It is a popular preprocessing step for later processing of the image, such as edge detection. In this technique, the gray level of each pixel is replaced by the median value of gray levels in the neighborhood pixels for a

given kernel size. The superiority of the Median filter over the 'average' filter is that any single unrepresentative pixel in the neighborhood cannot affect the median value. Hence, it is more robust compared to average filters. The median filter is much more useful to reduce impulsive or salt and pepper noise that happens due to random bit errors in a communication channel. For all pixels in a neighborhood of 'w', the following equation (11) can express the working principle,

$$I(k,l) = median\{x(i, j), (I, j)\epsilon w\} \tag{11}$$

'$I(k, l)$' represents the image obtained after filtering; '$x(i, j)$' are the pixels with '$(i, j)$' coordinates; '$w$' is the location, which is centered around the location $(k, l)$ of the image [37].

*c) Gaussian* (type: linear filter)-it blurs images and reduces the contrast. The *standard deviation* plays a crucial role in its behavior. The Gaussian filter works by calculating the probability distribution of the noise and then smoothening it by using its 2D distribution property (convolution) as a point spread function. There are also a few salient points, which are worth mentioning here, as (i) it is a non-uniform low-pass filter, (ii) the kernel coefficients decrease with increased distance from the kernel's center, (iii) central pixels have higher weightage than those in the periphery, (iv) larger values of standard deviation leads to wider or more stretched peaks and so the greater blurring, (v) as standard deviation increases, the kernel size also need to be increased to preserve the Gaussian nature of the function, (vi) kernel coefficients, therefore, depend on the value of standard deviation, (vii) at the edge of the blur, coefficient values should be close to zero, (viii) the kernel is rationally symmetric and hence is devoid of any type of skewness or directional bias, (ix) the kernel is separable and hence allows faster computation, and (x) it can preserve the contrast but not brightness. The formula of the Gaussian function in 1D and 2D is as shown in equations (12a) and (12b):

$$G_{(x)} = \frac{1}{\sqrt{2\pi\sigma^2}} e^{-\frac{x^2}{2\sigma^2}} \tag{12a}$$

In the case of 2D Gaussian, it is the product of two 1D Gaussians, one of each dimension, and is represented as follows,

$$G_{(x,y)} = \frac{1}{\sqrt{2\pi\sigma^2}} e^{-\frac{x^2+y^2}{2\sigma^2}} \tag{12b}$$

Where '$x$' and '$y$' represent horizontal and vertical axes, '$\sigma$' is the standard deviation of the Gaussian distribution. Values obtained from this distribution are used to build a convolutional matrix that in turn is applied to the original image. Each pixel's new value is then set to a weighted average of that pixel's neighborhood. The original pixels receive high weights (i.e., the high Gaussian value) and the neighborhood pixels receive lower values (i.e., smaller weights) as their distances from the original pixels increase. This operation, that's why results in the blurring of the image with edge preservation in a much better way [38].

*d) Bilateral* (type: non-linear filter)-it replaces the intensity of each pixel with a *weighted average* of the intensity values from nearby pixels, which is obtained from the Gaussian distribution. It can preserve the edges of the image. The weights are calculated based on Euclidean distance and Radiometric differences (e.g., color intensity, depth difference, etc.) of any two adjacent pixels. It can preserve sharp images. In case the range parameter (standard deviation) increases, Bilateral filtering gradually takes Gaussian convolution. The working principle is as follows equations (13a and 13b), respectively:

$$I^{(filtered)}(x) = \frac{1}{W_p} \sum_{x_i \in \Omega} I(x_i) f_r \left( \| I(x_i) - I(x) \| \right) g_s \left( \| x_i - x \| \right) \tag{13a}$$

$$W_p = \sum_{x_i} f_r \left( \sum_{x_i \in \Omega} I(x_i) f_r \left( \| I(x_i) - I(x) \| \right) g_s \left( \| x_i - x \| \right) \right) \tag{13b}$$

Where $I^{(filtered)}(x)$ refers to the filtered image and '$I$' is the original image to be filtered; '$x$' denotes the coordinates of the current pixels that need to be filtered; '$\Omega$' represents the window centered in '$x$', hence '$x \in \Omega$' is any pixel within that window; '$f_r$' represents the kernel range for smoothening differences in intensities and this can be a Gaussian function; '$g_s$' denotes the spatial kernel for smoothening differences in the coordinates and this can also be a Gaussian function; '$W_p$' is the weight value using spatial closeness; '$i, j$' is the coordinate value of the pixels (i.e., pixel locations), which needs to be denoised in an image using neighborhood pixels and one of its neighboring pixel is located at '$k$, $l$', and therefore assuming the range and spatial kernels to be Gaussian kernels, the weight assigned for pixel '$k, l$' to denoise pixel '$I, j$' is given by the following equation (13c):

$$W(i, j, k, l) = \exp \left( -\frac{(i-k)^2}{2\sigma_d^2} - \frac{\| I(x, j) - I(k, l) \|^2}{2\sigma_d^2} \right) \tag{13c}$$

Where, $\sigma_d$, $\sigma_r$ are the smoothing parameters and $I(i, j)$ and $I(k, l)$ are the intensity pixels $(i, j)$ and $(k, l)$, respectively. Finally, weights are *normalized* using equation (13d):

$$I_D(I, j) = \frac{\sum_{k,l} I(k,l) w(i, j, k, l)}{\sum_{k,l} w(i, j, k, l)} \tag{13d}$$

Where, '$I_D$' is the denoised intensity of the pixel $(i, j)$ [39].

Results of the original (Control, CXR Test-1, and CXR Test-2) can be seen in Table 3a-c and its corresponding filtered images can be viewed in Figure 5a-c, respectively.

## 3.7 *Performance testing*

It is desired that the images obtained by good filtering techniques should be less noisy. Hence, the performance of the individual filtering techniques is assessed by computing *Mean Squared Error (MSE)* and *Peak Signal-to-Noise Ratio (PSNR)*, which are popular techniques to estimate noise levels in a processed image [40-41].

*a) MSE*-represents the cumulative squared error between the denoised and original image (see equation 14). Hence, lower values are appreciated.

$$MSE = \frac{1}{m \cdot n} \sum_{i=0}^{m-1} \sum_{j=0}^{n-1} (I(i, j) - K(i, j))^2 \tag{14}$$

Where, '$m, n$' represents image matrix '$I(i, j)$' (original image) and '$K(i, j)$' (denoised image).

*b) PSNR*-represents the peak error of an image and is expressed as a ratio of peak or maximum signal value and the power of the distorting noise effect. Therefore, higher values are appreciated (refer to equation 15).

$$PSNR = 20 \log_{10}(MAX / (MSE)^{(1/2)}) \tag{15}$$

Where, *MAX* is the peak/maximum value of any pixel and *MSE* is the Mean Squared Error among pixels of original and denoised images. As mentioned before, Table 4a and b show the performance of the denoising techniques on original images by estimating MSE and PSNR.

*c) Computational time complexity (Big(O))*-has been estimated as another performance measure of how much time is required to get the output for the various denoising technique and original image combinations. Equation (16)

explains how Big(O) is computed (see equation 16),

$$Big(O) = (2n) \qquad (16)$$

Where, '*n*' is the number of pixels, which are counted twice during processing-once along the *x-axis* and then along the *y-axis* [42]. Table 5 shows the Big(O) values (in milliseconds) for all combinations. Figure 6 shows the corresponding plots.

*d) Prediction* of five hundred Tubercular CXRs has been attempted to examine the practical value of the Median, Gaussian, Bilateral, and Moving average filters in assisting the clinical diagnosis. To do so, the *statistical pixel features* of each denoised Tubercular image have been measured and stored as a CSV file, which is then divided into the training (75%) and test (25%) data sets. Using the principle of *k-means clustering*, mean-of-means (MOM) pixels of the training CXRs are computed as the centroid of the Tuberculosis cluster. Finally, the Euclidean distance (ED) of the pixel mean of each test CXR has been computed with a thresholding of 10%, which means if the ED falls below or equals 10%, the prediction is assumed to be *correct*. It is also important to note that before denoising, all images are resized as 224 × 224 pixels (mean size) as the images have a different size from each other due to differences in devices and acquisition parameters [43]. The best denoising algorithm could therefore be one that can give the least *loss-less images* following filtering and can retain the statistical feature of pixels.

# 4. Experimental results and discussions

In this section, results thus obtained by applications of various methods and techniques (already described in Section 3), have been shown and explained.

## 4.1 *Materials and method*

Three CXRs, one *normal* (Control) and two *abnormal/pathological* (Test CXR-1 and 2) have been acquired and their shapes are displayed in Figure 3. Proper *ethical measures* have been obtained throughout the acquisition process and patients' names, MRDs, and clinic sources have been kept anonymous throughout the study. It is important to note here that the reason for taking two different pathological and one normal CXR is just to bring some variety in the image quality (shape, size, pixel values, nature of data by descriptive statistics, skewness, etc.) and not used for any automatic prediction/classification or diagnostic purpose at this very stage.



Control (*240, 198, 3*)    Test CXR-1 (*135, 144, 3*)    Test CXR-2 (*138, 130, 3*)
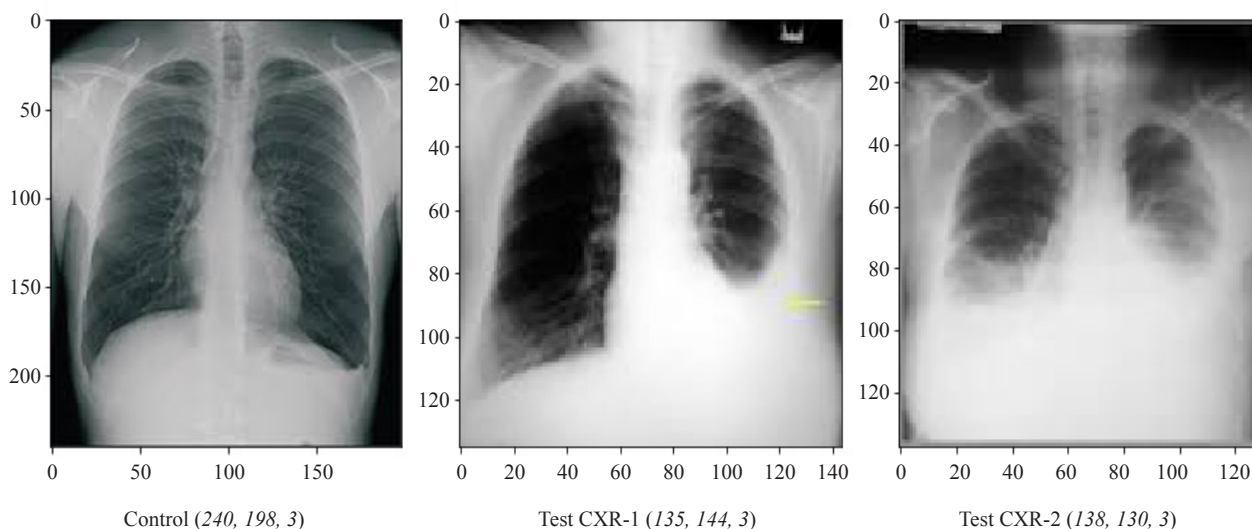
**Figure 3.** Three CXR images of adult males-Control (normal), Test CXR-1, and 2 (pathological).

## 4.2 *Feature extraction*

Observing the nature of data is a prerequisite of a data mining task. Descriptive statistics and the skewness of each image have been examined to understand the nature of the data. Table 2 shows the results obtained. It is observed that the distributions of the image data (normalized) are all negatively skewed (skewness_control = -0.279319, skewness_ CXR Test-1 = -0.625096, and skewness_CXR Test-2 = 0.608718). Although the size of CXR Test-1 and 2 are 10.32% different, compared to Control and CXR Test-1 and 2, the mean values of the pixels are almost the same (0.00016%). However, there is a considerable difference in the median value, which is 9.11%.

**Table 2.** Descriptive statistics and skewness of images

| | Actual | Normalized | | Actual | Normalized | | Actual | Normalized |
|---|---|---|---|---|---|---|---|---|
| Count | 47520 | 47520 | Count | 19440 | 19440 | count | 17940 | 17940 |
| Mean | 23759.5 | 0.4708566 | Mean | 9719.5 | 0.61082186 | mean | 8969.5 | 0.61071698 |
| Std | 13717.9 | 0.2200937 | Std | 5611.98 | 0.30884037 | std | 5178.97 | 0.26824191 |
| Min | 0 | 0.0005655 | Min | 0 | 0.00044565 | min | 0 | 0.00001211 |
| 25% | 11879.7 | 0.2855165 | 25% | 4859.75 | 0.35686274 | 25% | 4484.75 | 0.43137254 |
| 50% (median) | 23759.5 | 0.4871455 | 50% (median) | 9719.5 | 0.70980392 | 50% (median) | 8969.5 | 0.64509803 |
| 75% | 35639.2 | 0.6823529 | 75% | 14579.2 | 0.87843137 | 75% | 13454.2 | 0.87058823 |
| Max | 47519 | 0.8705882 | Max | 19439 | 0.93765647 | max | 17939 | 0.94509803 |
| Skewness | | -0.279319 | Skewness | | -0.625096 | skewness | | -0.608718 |
| Descriptive statistics-Control | | | Descriptive statistics-CXR Test-1 | | | Descriptive statistics-CXR Test-2 | | |

## 4.3 *Histogram equalization*

The histogram equalization (HE) technique has been applied to enhance the contrast of each image under study. Also to note whether HE has got any influence on the noise [44].

In Figure 4, *intensity/frequency values* of the enhanced images are just over 500, 200, and 400 for Control, Test CXR-1, and Test CXR-2, respectively along the y-axis. Along x-axes, *pixel values* of Control CXR range from 0 to just over 200. While for CXR Test-1 and Test-2, it is stretched up to 250, in each, respectively. The blue line indicates the corresponding *cdf* post-equalization transform of relabeled pixels. It ranges from the origin (0,0) to the high-frequency points that represent contrast-enhanced portions in the images.
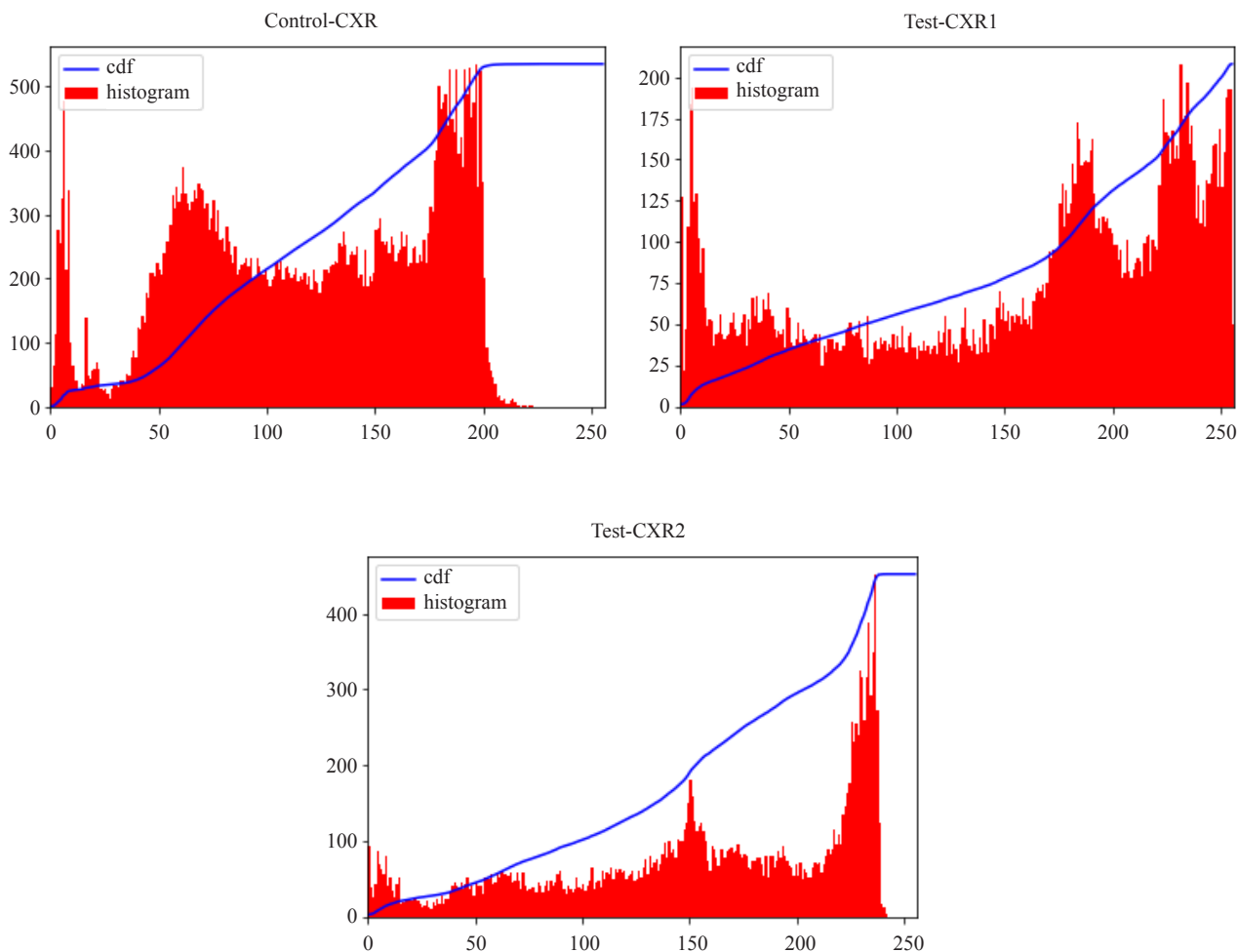
**Figure 4.** Histogram equalization of three CXR images

## 4.4 *Noise detection*

Noise in the images has been assessed using *SNR* and *Noise variance* estimations, at first on 'raw acquired images' and then 'histogram equalized images. It is important to mention here that, in this work, no specific type of noise has been detected. Results of Noise variance and SNR for each of the images can be seen below in Table 3a and 3b, respectively.

**Table 3a.** Noise detected in raw images

| Original Image (raw) | Noise_var | SNR_min | SNR_max | SNR_mean | SNR_median | SNR_std |
|---|---|---|---|---|---|---|
| *Control (240, 198)* | 0.1031 | 0.931 | 9.5008 | 2.8994 | 2.3022 | 1.9005 |
| *CXR Test-1 (135, 144)* | 0.1015 | 0.945 | 26.6015 | 5.0053 | 2.5994 | 6.4016 |
| *CXR Test-2 (138, 130)* | 0.1019 | 1.402 | 68.2351 | 3.5119 | 2.3123 | 6.8049 |

| Original Image (post HE) | Noise_var | SNR_min | SNR_max | SNR_mean | SNR_median | SNR_std |
|---|---|---|---|---|---|---|
| *Control (240, 198)* | 0.1029 | 0.936 | 9.5103 | 2.9194 | 2.3426 | 1.9095 |
| *CXR Test-1 (135, 144)* | 0.1010 | 0.958 | 26.6205 | 5.0353 | 2.6244 | 6.4086 |
| *CXR Test-2 (138, 130)* | 0.1023 | 1.442 | 68.2741 | 3.5449 | 2.3674 | 6.8069 |

From Table 3, it can be noted that the best image (i.e., least noisy) is Control CXR (noise variance = 0.1031, average SNR = 2.8994, and median SNR = 2.3022 before HE). The cells are highlighted and marked with yellow color. After HE, the noise variance is 0.1029, average SNR = 2.9194, and median SNR = 2.3426, where the cells are highlighted and marked as orange color (deeper shades as the noise increases). It can be noted that HE has increased the noise level by 1%, probably by raising the contrast background noise, while decreasing the usable signal. Therefore, denoising/filtering techniques are used on the original CXR images and not on HE-applied images.

## 4.5 *Denoising of the original images*

Four filtering/denoising techniques have been used on these three CXR plates, such as *Moving average*, *median*, *Gaussian*, and *Bilateral*. The detail of each has already been discussed in Section 3. Below are the output (i.e., filtered) images and the original images.

a) Original Vs. Filtered Images (Control CXR)
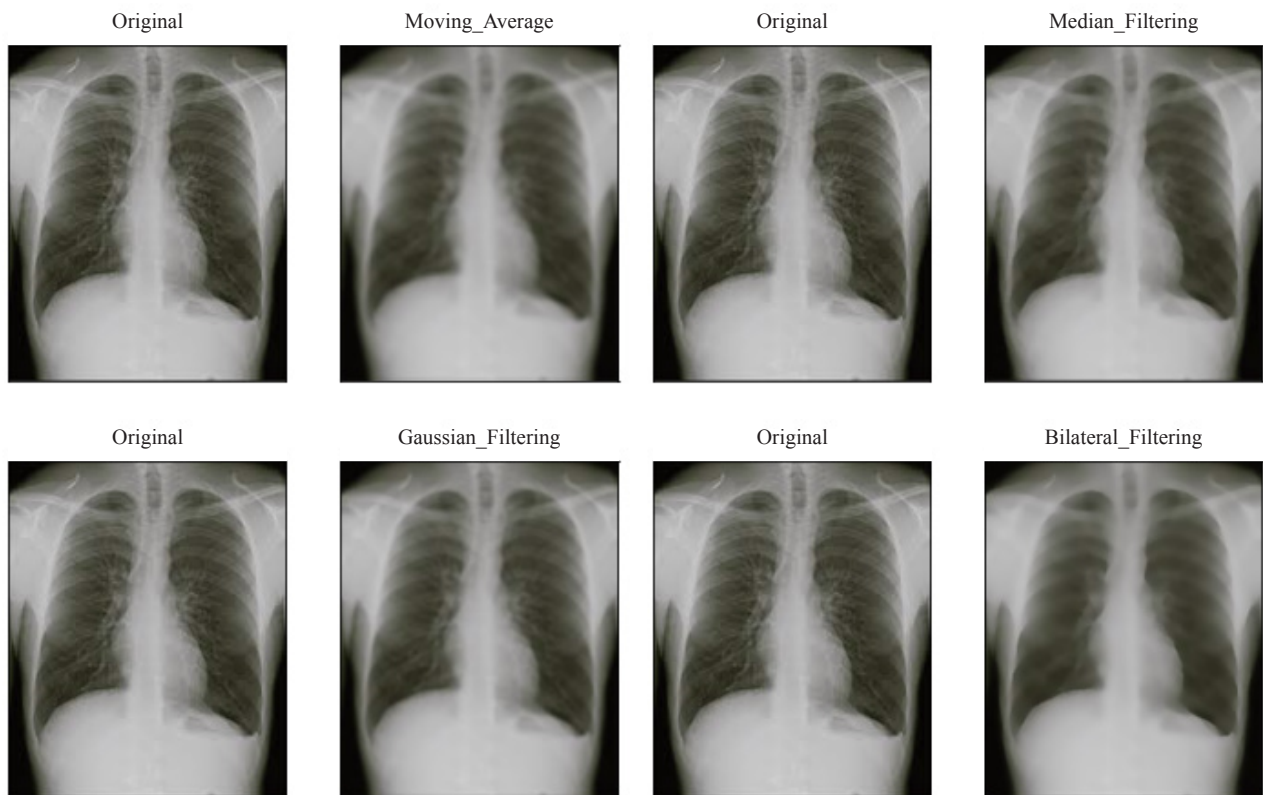


**Figure 5a.** Control images-original vs. filtered

b) Original Vs. Filtered Images (Test CXR-1)



| Original | Moving_Average | Original | Median_Filtering |

| Original | Gaussian_Filter | Original | Bilateral_Filter |
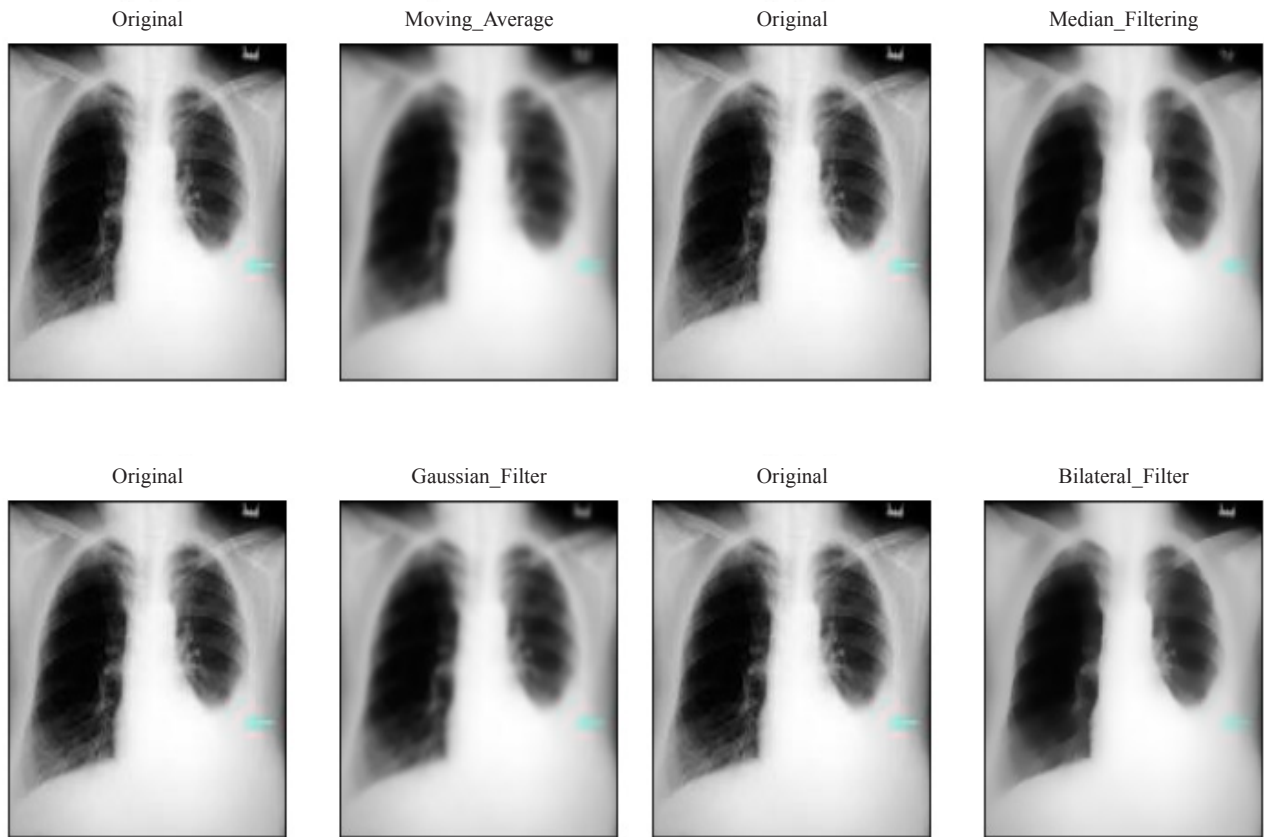
**Figure 5b.** CXR Test-1 image-original vs. filtered

c) Original Vs. Filtered Images (Test CXR-2)



| Original | Moving_Average | Original | Median_Filtering |
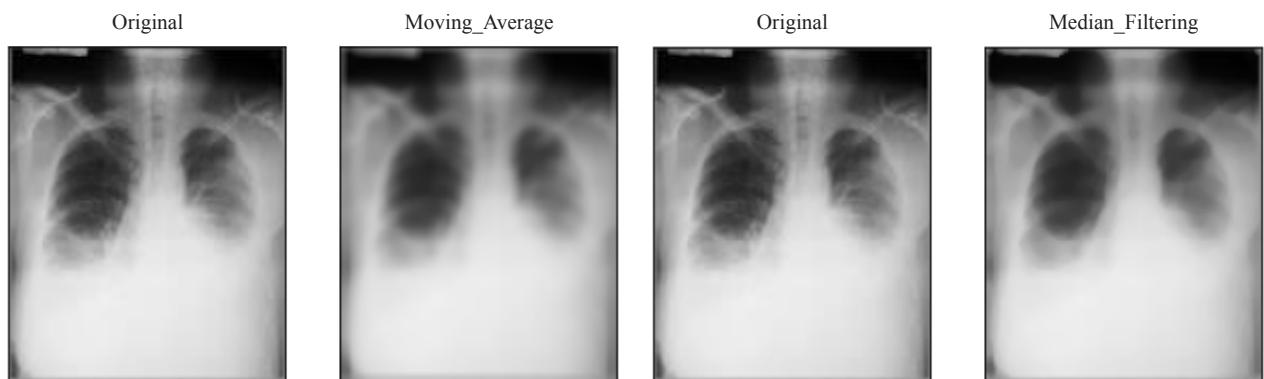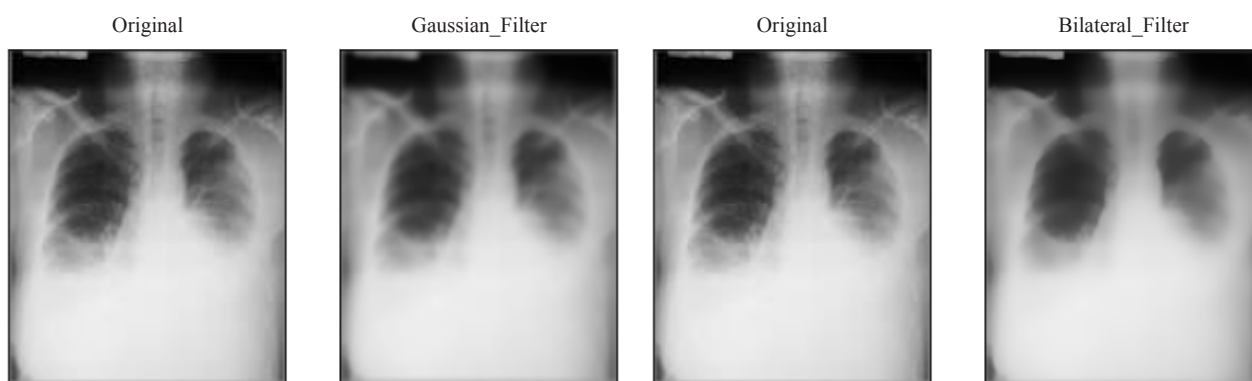
**Figure 5c.** CXR Test-2 image-original vs. filtered

After filtering, at first, the *Noise variance* and *SNR* of the images have been estimated, followed by testing the performance of the filtering techniques by computing the *MSE* and *PSNR* scores of the said images.

## 4.6 *Assessment of quality of filtering*

It is assessed by first measuring the *Noise variance* and *SNR* (see Table 4a, 4b, and 4c) and then by computing *MSE* and *PSNR* values (refer to Table 5a and 5b) of each of the filtered images.

**Table 4a.** Noise estimation of filtered image (Control)

| Filtered Image (Control) | Noise_var | SNR_min | SNR_max | SNR_mean | SNR_median | SNR_std |
|---|---|---|---|---|---|---|
| *Moving_avg* | 0.0993 | 0.9830 | 9.4786 | 2.9783 | 2.3830 | 1.9508 |
| *Median* | 0.1027 | 0.9956 | 9.3782 | 2.9555 | 2.3677 | 1.9328 |
| *Gaussian* | 0.0994 | 0.9756 | 9.7145 | 2.9669 | 2.3612 | 1.9624 |
| *Bilateral* | 0.1014 | 0.9940 | 9.0543 | 2.9901 | 2.4092 | 1.9308 |

**Table 4b.** Noise estimation of filtered image (CXR Test-1)

| Filtered Image (CXR Test-1) | Noise_var | SNR_min | SNR_max | SNR_mean | SNR_median | SNR_std |
|---|---|---|---|---|---|---|
| *Moving_avg* | 0.0992 | 0.9765 | 26.4222 | 5.0923 | 2.6731 | 6.3647 |
| *Median* | 0.1192 | 0.9677 | 26.6052 | 5.0888 | 2.6504 | 6.4878 |
| *Gaussian* | 0.0964 | 0.9685 | 26.5792 | 5.0752 | 2.6722 | 6.3955 |
| *Bilateral* | 0.0974 | 0.9849 | 25.9258 | 5.1072 | 2.6974 | 6.3294 |

**Table 4c.** Noise estimation of filtered image (CXR Test-2)

| Filtered Image (CXR Test-2) | Noise_var | SNR_min | SNR_max | SNR_mean | SNR_median | SNR_std |
|---|---|---|---|---|---|---|
| *Moving_avg* | 0.1006 | 1.4586 | 5.8424 | 2.8159 | 2.3747 | 1.2149 |
| *Median* | 0.1013 | 1.4477 | 93.4729 | 2.4931 | 2.3502 | 9.9695 |
| *Gaussian* | 0.1007 | 1.4565 | 9.1129 | 2.8601 | 2.3628 | 1.4034 |
| *Bilateral* | 0.0993 | 1.4683 | 7.6975 | 2.8402 | 2.3826 | 1.2867 |

For all CXRs (Control, CXR Type-1, and CXR Type-2), the *Median filter* has outperformed its competitors, such as Moving average, Gaussian, and Bilateral filtering techniques, observed from a-c with average (Noise variance = 0.1073, SNR mean = 3.5124, and SNR median = 2.4561).

Then MSE and PSNR values are estimated to test the filtering performance (Table 5a-b, respectively). it is noted that the average MSE (12.2337) is the least for the *Median filter* (Med_filt), closely followed by the Gaussian filter (average MSE = 12.6062). PSNR shows a similar result, i.e., the *Median filter* (Med_filt) is the best of the lot, closely followed by the Gaussian filter (average PSNR = 34.5213 and 33.9924, respectively).

**Table 5a.** MSE of filtered images

| Original Image | Moving_avg | *Med_filt* | Gauss_filt | Bilat_filt |
|---|---|---|---|---|
| *Control (240, 198)* | 22.0976 | 13.9699 | 12.6138 | 26.8809 |
| *Test1 (135, 144)* | 22.625 | 11.7383 | 12.5888 | 26.6119 |
| *Test2 (138, 130)* | 21.0355 | 10.9929 | 13.2159 | 27.0693 |
| *Average* | 21.9194 | 12.2337 | 12.8062 | 26.8540 |
| *Standard deviation* | 0.8096 | 1.5491 | 0.3551 | 0.2299 |

**Table 5b.** PSNR (dB) of filtered images

| Original Image | Moving_avg | *Med_filt* | Gauss_filt | Bilat_filt |
|---|---|---|---|---|
| *Control (240, 198)* | 32.2517 | 35.616 | 34.9328 | 31.6817 |
| *Test1 (135, 144)* | 31.7725 | 33.8001 | 35.5053 | 31.6851 |
| *Test2 (138, 130)* | 27.7098 | 34.1479 | 31.539 | 29.4483 |
| *Average* | 30.578 | 34.5213 | 33.9924 | 30.9384 |
| *Standard deviation* | 2.4955 | 0.9638 | 2.1439 | 1.2904 |

Table 6 shows the *Big(O)* values computed for all combinations as follows. It can be noted that the Median filter takes the least computational time (average time of 0.02873 milliseconds), which means that the *Median filter* is 76%, 67.8%, and 57.8% more efficient than that of Moving average, Gaussian, and Bilateral denoising techniques. The reason could be its most simplistic approach of calculating the median and replacing the neighborhood pixels with it in an iterative manner till all pixels are covered. Another important cause could be that it is not influenced by entropies (highly dissimilar values) in the pixels and last but not least, it works well in the Poisson type of noise that is a common occurrence in CXRs. CXR image production uses photon-counting statistics that follow the Poisson process. Thus, the noise present in the CXR has the Poisson distribution and the noise is called the Poisson noise or Shot noise [45].

**Table 6.** Calculated Big(O) values (millisecond)

| Original CXR Image | Moving_avg | Median | Gaussian | Bilateral |
|---|---|---|---|---|
| *Control (240, 198)* | 0.0511 | 0.0461 | 0.064 | 0.0658 |
| *CXR Test1 (135, 144)* | 0.0313 | 0.0201 | 0.0348 | 0.0488 |
| *CXR Test2 (138, 130)* | 0.0281 | 0.02 | 0.0282 | 0.0293 |
| *Average* | *0.03417* | *0.02873* | *0.04233* | *0.04797* |
| *Stdev* | *0.01570* | *0.01504* | *0.01905* | *0.01826* |

Figure 6 shows the *Big(O)* for all image-technique combinations. Trendlines are added over pivot highs of each line plot for Control, CXR Test-1, and CXR Test-2 to see the prevailing direction of the time complexities. It can be noted that it is linear to algorithmic complexities and pixel size of the images.
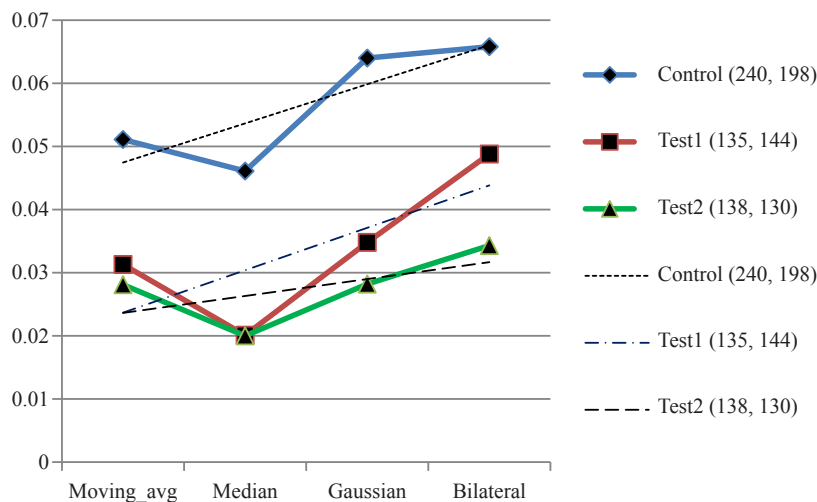


**Figure 6.** Time complexity plots and the respective trendlines

Finally, to examine the real-world value of these filters, the filtered images are tested for *predicting* five hundred Tubercular CXRs. The ED between the mean pixel value for Tubercular CXR and the mean pixel value of the

Tubercular test image show < 0.1 (considering a 10% cutoff value, i.e., there must be a 90% match). Using the Median filter, 92% CXRs are accurately diagnosed, followed by Gaussian, Bilateral, and Moving averages showing accuracy values of 80%, 72%, and 60%, respectively.

## 5. Conclusions and future research

Denoising an image is an important pre-processing step in an image processing task. There are several denoising techniques available. In this work, four popular techniques such as Moving average, median, Gaussian, and Bilateral filters have been applied on a set of CXRs-one considered to be 'within normal limits and the remaining two as 'pathological'. Extensive experimentation has been conducted to examine the denoising performances of these techniques by estimating *Noise variance*, *SNR*, *MSE*, *PSNR*, and *Big(O)*. For each image, the *Median filtering* technique has outperformed its competitors by reducing noise and preserving important signals, as corroborated by *higher* Noise variance, SNR, PSNR values, and *lower* MSE, Big(O) values, and in predicting Tubercular test CXRs. The reason could be due to the occurrence of Poisson-type noise in X-ray images, where the Median filter works well [10, 46].

The *contribution* of this work lies in its comprehensive research on applications of various denoising techniques to find out the best of the lot for 2D CXR image filtering. It could be a ready reckoner for future researchers to choose a Median filter as an appropriate denoising technique for such images and hence, can be time-saving.

The limitations of this work are (i) less number of CXR images and (ii) other denoising methods that have been skipped as those were not the focus of this work and can be pursued as future work.

## Conflict of interest

The author affirms that there is no conflict of interest.

## References

[1] Clarence R, Devanathan M, Ahmed RZ. Investigation of various noise and denoise methods in satellite images. *International Journal of Advanced Science and Technology*. 2020; 29(10s): 7734-7740.

[2] Selami AMA, Fadhil AF. A study of the effects of gaussian noise on image features. *Kirkuk University Journal/ Scientific Studies (KUJSS)*. 2016; 11(3): 152-169.

[3] Owotogbe JS, Ibiyemi TS, Adu BA. A comprehensive review on various types of noise in image processing. *International Journal of Scientific & Engineering Research*. 2019; 10(11): 388-393.

[4] Liang S, Liu H, Gu Y, Guo X, Li H, Li L, et al. Fast automated detection of COVID-19 from medical images using convolutional neural networks. *Communications Biology*. 2021; 4(1): 1-13.

[5] Chattopadhyay S. A novel approach to detect abnormal chest X-rays of COVID-19 patients using image processing and deep learning. *Artificial Intelligence Evolution*. 2021; 2(2): 23-41.

[6] Chattopadhyay S. An approach to identify the regions of interest in chest X-ray images of COVID-19 patients and its clinical validation. *Artificial Intelligence Evolution*. 2022; 3(1): 41-54.

[7] Singh P, Bose SS. Ambiguous D-means fusion clustering algorithm based on ambiguous set theory: Special application in clustering of CT scan images of COVID-19. *Knowledge-Based Systems*. 2021; 231: 107432.

[8] Singh P, Bose SS. A quantum-clustering optimization method for COVID-19 CT scan image segmentation. *Expert Systems with Applications*. 2021; 185: 115637.

[9] Smith-Bindman R, Miglioretti DL, Larson EB. Rising use of diagnostic medical imaging in a large integrated health system. *Health Affairs*. 2008; 27: 1491-1502.

[10] Thakur K, Kadam J, Sapkal A. Poisson noise reduction from X-ray images by region classification and response median filtering. *Sadhana*. 2017; 42(6): 855-863.

[11] Rawat W, Wang Z. Deep convolutional neural networks for image classification: a comprehensive review. *Neural Computing*. 2017; 29: 2352-2449.

[12] Zeng Y, Zhang B, Zhao W, Xiao S, Zhang G, Ren H, et al. Magnetic resonance image denoising algorithm based on

cartoon, texture, and residual parts. *Computational and Mathematical Methods in Medicine*. 2020; 2020: 1405647. Available from: https://doi.org/10.1155/2020/1405647.

[13] Sun Y, Xue B, Zhang M, Yen GG. Evolving deep convolutional neural networks for image classification. *IEEE Transactions of Evolving Computing*. 2019; 24: 394-407.

[14] Alisha PB, Sheela KG. Image denoising techniques-An overview. *Journal of Electronics and Communication Engineering*. 2016; 11(1): 78-84.

[15] Clouet A, Vaillant J, Alleysson D. The geometry of noise in color and spectral image sensors. *Sensors*. 2020; 20(16): 4487.

[16] Rong Z, Wang Y. Application of improved median filter on image processing. *Journal of Computers*. 2012; 7(4): 838-841.

[17] Kwon S, Kim D, Han B, Kwon K. Regularization of DT-MRI using 3D median filtering methods. *Journal of Applied Mathematics*. 2014; 2014(SI05): 1-11.

[18] Suhas S, Venugopal CR. MRI image preprocessing and noise removal technique using linear and nonlinear filters. *2017 International Conference on Electrical, Electronics, Communication, Computer, and Optimization Techniques (ICEECCOT)*. IEEE; 2017. p.1-4.

[19] Ali HM. MRI Medical image denoising by fundamental filters. In: Halefoğlu AM. (ed.) *High-Resolution Neuroimaging-Basic Physical Principles and Clinical Applications*. Turkey: Intechopen; 2018. p.111-124.

[20] Shlykov V, Kotovskyi V, Višniakov N, Šešok A. Model for elimination of mixed noise from MRI heart images. *Applied Sciences*. 2020; 10(14): 4747.

[21] Selvi PM, Ashadevi V. Elimination of noise in CT images of lung cancer using image preprocessing filtering techniques. *International Journal of Advanced Science and Technology*. 2020; 29(4): 1823-1832.

[22] Li H, Zhao J, Xu S, Cui Y. Combined noise reduction in CT-image based on adaptive median filter and wavelet packet. In: Dai M. (ed.) *Innovative Computing and Information. International Conference on Information and Management Engineering*. Wuhan, China: Springer, Berlin, Heidelberg; 2011. p.550-557.

[23] Abdullah MF, Sulaiman SN, Osman MK, Karim NKA, Shuaib IL, Alhamdu MDI. Classification of lung cancer stages from CT scan images using image processing and k-nearest neighbours. *11th IEEE Control and System Graduate Research Colloquium (ICSGRC)*. IEEE; 2020. p.68-72.

[24] Paul EM, Perumal B, Rajasekaran MP. Filters used in X-ray chest images for initial stage tuberculosis detection. *2018 International Conference on Inventive Research in Computing Applications (ICIRCA)*. Coimbatore, India: IEEE; 2018. p.235-239.

[25] Huang RY, Dung LR, Chu CF, Wu YY. Noise removal and contrast enhancement for X-ray images. *Journal of Biomedical Engineering and Medical Imaging*. 2016; 3(1): 56.

[26] Hu S, Liao Z, Chen W. Reducing noises and artifacts simultaneously of low-dosed X-ray computed tomography using bilateral filter weighted by gaussian filtered sinogram. *Mathematical Problems in Engineering*. 2012; 2012: 138581. Available from: https://doi.org/10.1155/2012/138581.

[27] Shinde B, Dani AR. Noise detection and removal filtering techniques in medical images. *International Journal of Engineering Research and Applications*. 2012; 2(4): 311-316.

[28] Turceryan M, Jain AK. Texture analysis. In: Chen CH, Pau LF, Wang PSP. (eds.) *Handbook of Pattern Recognition and Computer Vision*. Singapore. World Scientific Publishing; 1993. p. 235-276.

[29] Humeau-Heurtier A. *Texture feature extraction methods: A survey*. IEEE Access; 2019. p.8975-9000.

[30] Chattopadhyay S, Choudhuri SB. Automatic grading of premenstrual syndrome: Simulating the manual diagnosis process. *American Journal of Biomedical Engineering*. 2016; 6(3): 78-85.

[31] Kardian AR, Sudiro SA, Madenda S. Efficient implementation of mean, variance and skewness statistic formula for image processing using FPGA device. *Bulletin of Electrical Engineering and Informatics*. 2018; 7(3): 386-392.

[32] Dorothy R, Joany RM, Rathish RJ, Prabha SS, Rajendran S. Image enhancement by histogram equalization. *International Journal of Nano Corrosion Science and Engineering*. 2015; 2(4): 21-30.

[33] Mohapatra BN, Panda PP. Histogram equalization and noise removal process for enhancement of image. *Transactions on Image Processing and Computer Vision*. 2020; 3(9): 2455-4707.

[34] School of Physics and Astronomy. The University of Edinburgh; 2007. Available from: https://www2.ph.ed.ac.uk/; https://www2.ph.ed.ac.uk/~wjh/teaching/dia/documents/noise.pdf [Accessed 23th April 2021].

[35] Swamy S, Kulkarni PK. A basic overview on image denoising techniques. *International Research Journal of Engineering and Technology (IRJET)*. 2020; 7(5): 850-857.

[36] Finch T. *Incremental calculation of weighted mean and variance*. 2009. p.1-8. Available from: https://fanf2.user.srcf.net/hermes/doc/antiforgery/stats.pdf.

[37] hmc.edu. 2019. Available from: http://fourier.eng.hmc.edu; http://fourier.eng.hmc.edu/e161/lectures/smooth_

sharpen/node2.html [Accessed 25th April 2021].

[38] Haddad RA, Akansu AN. A class of fast gaussian binomial filters for speech and image processing. *IEEE Transactions on Acoustics, Speech, and Signal Processing*. 1991; 39: 723-727.

[39] Banterle F, Corsini M, Cignoni P, Scopigno R. A low-memory, straightforward and fast bilateral filter through subsampling in spatial domain. *Computer Graphics Forum*. 2011; 31(1): 19-32.

[40] Dabas P, Mehra R. Estimation of the image quality under different distortions. *International Journal of Advanced Trends in Computer Science and Engineering*. 2016; 8(7): 17291-17296.

[41] Jemila SJ, Therese AB. Selection of suitable segmentation technique based on image quality metrics. *The Imaging Science Journal*. 2019; 67(8): 475-480.

[42] Schellekens J. Stack overflow. 2019. Available from: https://stackoverflow.com/; https://stackoverflow.com/questions/55438638/how-to-find-computation-complexity-of-image-processing-algorithm#:~:text=As%20a%20rough%20measure%2C%20you,viewed%2Fedited%20by%20the%20algorithm.&text=Its%20complexity%20is%20O(n,pixels%20in%20the%20input%20im [Accessed 17th April 2021].

[43] Wang D, Mo J, Zhou G, Xu L, Liu Y. An efficient mixture of deep and machine learning models for COVID-19 diagnosis in chest X-ray images. *PloS One*. 2020; 15(11): e0242535.

[44] ece.ubc.ca. Histogram Equalization. Available from: http://www.ece.ubc.ca/~irenek/techpaps/introip/manual02.html#:~:text=Histogram%20equalization%20can%20be%20done,image%20to%20an%20output%20image [Accessed 22th April 2021].

[45] Thakur KV, Damodare OH, Sapkal AM. Poisson noise reducing bilateral filter. *Procedia Computer Science*. 2016; 79: 861-865.

[46] Shah A, Bangash JI, Khan AW, Ahmed I, Khan A, Khan A, et al. Comparative analysis of median filter and its variants for removal of impulse noise from gray scale images. *Journal of King Saud University-Computer and Information Sciences*. 2022; 34(3): 505-519.